Project No. 11-2979

Development of Multiscale Materials Modeling Techniques and Coarse-Graining Strategies for Predicting Materials Degradation in Extreme Irradiation Environments

Reactor Concepts

Brian Wirth
University of Tennessee at Knoxville

In collaboration with:
None

Rob Versluis, Federal POC
Xin Sun, Technical POC

NEUP Nuclear Energy University Programs
U.S. Department of Energy

FINAL REPORT FOR
U.S. DEPARTMENT OF ENERGY NUCLEAR ENERGY UNIVERSITY PROGRAMS
Project 11-2979

Project Title: Development of Multiscale Materials Modeling Techniques and Coarse-Graining Strategies for Predicting Materials Degradation in Extreme Irradiation Environments

Technical Work Scope: ARC-3

Papers and Publications:

T.R. Allen, D. Kaoumi, J.P. Wharry, Z. Jiao, C. Topbasi, A. Kohnert, L. Barbard, A. Certain, K.G. Field, G.S. Was, D. Morgan, A.T. Motta, B.D. Wirth, and Y. Yang, "Characterization of Microstructure and Property Evaluation in Advanced Cladding and Duct: Materials exposed to high dose and elevated temperature", *Journal of Materials Research* **30** (2015) 1246-1274.

BD Wirth, X. Hu, A. Kohnert, and D. Xu, "Modeling Defect Cluster Evolution in Irradiated Structural Materials: Focus on comparing to high-resolution experimental characterization studies", *Journal of Materials Research* **30** (2015) 1440-1455.

A.A. Kohnert and B.D. Wirth, "Cluster dynamics models of irradiation damage accumulation in ferritic iron. II. Effects of reaction dimensionality", *Journal of Applied Physics* **117** (2015) 154306.

A.A. Kohnert and B.D. Wirth, "Cluster dynamics models of irradiation damage accumulation in ferritic iron. I. Trap mediated cluster diffusion", *Journal of Applied Physics* **117** (2015) 154305.

X. Hu, D. Xu, T.S. Byun, and B.D. Wirth, "Modeling of Irradiation Hardening of Iron after Low Dose and Low Temperature Neutron Irradiation", *Modeling and Simulation in Materials Science & Engineering* **22** (2014) 0655002.

D. Xu, B.D. Wirth, M. Li, and M. A. Kirk, "Defect Microstructural Evolution in Ion Irradiated Metallic Nanofoils: Kinetic Monte Carlo Simulation versus Cluster Dynamics Modeling and In-Situ TEM Experiments", *Applied Physics Letters* **101** (2012) 101905.

D. Xu, B.D. Wirth, M. Li and M.A. Kirk, "Combining in situ transmission electron microscopy irradiation experiments with cluster dynamics modeling to study nanoscale defect agglomeration in structural metals", *Acta Materialia* **60** (2012) 4286-4302.

M. Li, M.A. Kirk, P.M. Baldo, D. Xu, and B.D. Wirth, "Study of Defect Evolution by TEM with *in situ* Ion Irradiation and Coordinated Modelling", *Phil Mag* **92(no. 16)** (2012) 2048-2078.

Invited & Contributed Oral Presentations:

B.D. Wirth, X. Hu, A. Kohnert, and D. Xu, "Modeling Defect Cluster Evolution in Irradiated Structural Materials: Focus on irradiation type & comparing to high-resolution

characterization studies", 2015 Oxford University Irradiation Effects Workshop, Oxford, UK, 23 September 2015.

B.D. Wirth, X. Hu, A. Kohnert, and D. Xu, "Multiscale Modeling of Defect Cluster Evolution in Irradiated Structural Materials: Focus on comparing to high resolution characterization studies", Spring MRS Meeting, Symposium XX, San Francisco, CA, 7 April 2015.

B.D. Wirth, X. Hu, A. Kohnert, and D. Xu, "Multiscale Modeling of Defect Cluster Evolution in Irradiated Structural Materials: Focus on comparing thin-film, in-situ ion to neutron irradiation", 7th International Conference on Multiscale Materials Modeling, Symposium D, Berkeley, CA, 8 October 2014.

B.D. Wirth, A. Kohnert, X. Hu, and D. Xu, "Multiscale Modeling of Defect Cluster Evolution in Irradiated Structural Materials: Focus on comparing thin film, in-situ ion to neutron irradiation", TMS 2014 annual meeting Symposium on Accelerated Materials Evaluation for Nuclear Application, San Diego, CA, 18 February 2014.

B.D. Wirth, D. Xu, A. Selby, P. Baldo, M. Kirk, M.-M. Li, "Multiscale Modeling Radiation Damage and Damage Accumulation in Thin Metal Films: Comparison to In-Situ TEM Observation", Workshop on Materials in Extreme Environments, Michigan State University, 13 May 2013.

B.D. Wirth, A. Kohnert, A. Selby, and D. Xu, "Multiscale Modeling of Defect Cluster Evolution in Irradiated Structural Materials: Focus on thin-film, in-situ IVEM irradiation conditions", TMS 2013 Symposium on Microstructural Processes in Irradiated Materials, San Antonio, TX, 4 March 2013.

B.D. Wirth, D. Xu, A. Selby, P. Baldo, M. Kirk, and M.-M. Li, "Multiscale Modeling of Radiation Damage and Defect Accumulation Kinetics during Thin-Film Irradiation of Molybdenum: Comparison to In-Situ TEM Observation", Electron Microscopy Center Review, Argonne National Laboratory, 18 July 2012.

1. INTRODUCTION

Exposure of metallic structural materials to irradiation environments results in significant microstructural evolution, property changes and performance degradation, which limits the extended operation of current generation light water reactors and restricts the design of advanced fission and fusion reactors [1-8]. This effect of irradiation on materials microstructure and properties is a classic example of an inherently multiscale phenomenon, as schematically illustrated in Figure 1a. Pertinent processes range from the atomic nucleus to structural component length scales, spanning more than 15 orders of magnitude. Time scales bridge more than 22 orders of magnitude, with the shortest being less than a femtosecond [1,8]. Further, the mix of radiation-induced features formed and the corresponding property degradation depend on a wide range of material and irradiation variables. This emphasizes the importance of closely integrating models with high-resolution experimental characterization of the evolving radiation-damaged microstructure, including measurements performed in-situ during irradiation. In this article, we review some recent successes through the use of closely coordinated modeling and experimental studies of the defect cluster evolution in irradiated body-centered cubic materials, followed by a discussion of outstanding challenges still to be addressed, which are necessary for the development of comprehensive models of radiation effects in structural materials.

At the smallest scales (nanometer and picosecond), radiation damage continually initiates with the creation of energetic primary knock-on atoms in (primarily) elastic collisions between high-energy neutrons and lattice atoms [1,8]. Specifically for fusion conditions, there is also the production of high concentrations of transmutants, including insoluble He and H gas, produced in (n,α) and (n,p) neutron capture reactions, many of which have threshold energies above several MeV and thus are not typically produced in fission neutron irradiations [2-5]. The

primary knock-on atoms and recoiling transmutant nuclei quickly lose their kinetic energy in a chain of subsequent atomic collision displacements, generating a cascade of vacancy and self-interstitial defects. High-energy displacement cascades evolve over very short times, ~ 100 picoseconds or less, and small volumes, with characteristic length scales of 50 nm or less, and are directly amenable to molecular dynamics (MD) simulations. The physics of primary damage production in high-energy displacement cascades has been extensively studied with MD simulations [8-13]. The key conclusions of the high-energy (> 20 keV) simulations are that i) intra-cascade recombination of vacancies and self-interstitial atoms (SIA) results in ~30% of the defect production expected from displacement theory, ii) many-body collision effects produce a spatial correlation (separation) of the vacancy and self-interstitial defects, iii) substantial clustering of the self-interstitials and to a lesser extent, the vacancies occurs within the cascade volume, and iv) high-energy displacement cascades tend to break up into lobes, or sub-cascades which may also enhance recombination.

Spatial correlations continue to play an important role in nano/microstructural development, as the defects produced in the cascade at 100 ps evolve, or age, over much longer time scales [1,8]. The cascade aging evolution is governed by the time and temperature dependent kinetics of defect diffusion, clustering and annihilation. Fortunately, separation between the diffusion time scales of vacancies and SIA/SIA clusters naturally leads to the nearly independent evolution of these two populations, at least for relatively low dose rates and low doses, before cascade overlap becomes important. For example, numerous MD studies have shown that the SIA clusters in body-centered cubic iron are directly produced in high-energy displacement cascades and undergo one-dimensional glide with very low activation energies of ≤ 0.1 eV [14-16]. This low activation energy is contrasted to a value about 0.25 eV for individual

self-interstitial atoms and a value between about 0.6 and 1.0 eV for vacancies. Thus, mobile loops and isolated self-interstitials quickly diffuse through the vacancy debris and leave the cascade region. The additional vacancy - self-interstitial re-combination that occurs during this phase of cascade aging has been modeled with kinetic Monte Carlo methods [17].

The evolution of the remaining vacancy rich cascade core in Fe, and more recently in tungsten, has also been modeled by kinetic Monte Carlo methods [17-21], in the limit of infinitesimal dose rate. Within ms, most of the cascade vacancies jump short distances to form small, compact three-dimensional clusters, while a small fraction leave the cascade region. Subsequently, the vacancy clusters migrate, coarsen and ultimately dissolve. Reduction of the net residual vacancy concentration in the cascade core by emission-migration-annihilation events was observed to be essentially continuous in the model, but progressively slowed with cluster growth. Vacancy clusters initially grew through the coalescence of smaller mobile clusters, and later by emission-absorption processes. Notably, the formation of small (10-30) vacancy clusters, which are not visible in the TEM, has been confirmed in positron annihilation spectroscopy measurements in Fe and Fe-Cu alloys irradiated at temperatures below ~300°C [22,23].

The vacancy mediated cascade aging described in the preceding paragraph is limited to infinitesimal dose-rates and intermediate to low irradiation temperatures around 300°C. Clearly, the timescale associated with vacancy cluster coarsening and dissolution processes, as well as the assumption related to separation of the SIA/vacancy evolution timescales depends on the details of point defect interactions with solutes, impurities, precipitate interfaces, and extended defects like dislocations, in addition to depending strongly on irradiation temperature. As but one example, solute/impurity binding with small vacancy clusters and the segregation of chemical impurities (including He and possibly also hydrogen) to the surface of larger nanovoids leads to

increased vacancy cluster/nanovoid thermal stability. A quantitative assessment of vacancy/nanovoid-impurity complex lifetime, in particular with He and/or H transmutants, and the coupled interactions amongst point defect clusters, solutes, impurities and extended defects within the higher operating temperatures proposed for advanced fission reactors and in the fusion environment remains an outstanding issue.

Ultimately, long-range diffusion of vacancy and self-interstitial defects that escape the cascade region is responsible for nano/microstructural evolution. Enhanced defect transport leads to a re-distribution of solute and impurity elements as a consequence of radiation enhanced diffusion and segregation. Solute re-distribution can alter the local chemistry and result in the precipitation of phases not expected within a homogeneously distributed alloy. Outstanding questions relate to the effect of cascade aging processes on the fraction of defects contributing to long-range diffusion; the interaction of diffusing defects with continuously generated cascade debris; the modification of defect clustering and diffusion processes as a result of interactions with an evolving underlying nano/microstructure; and the efficiency of various microstructural sinks (including dislocations, grain boundaries, nanoscale precipitate interfaces and defect clusters themselves) in point defect cluster annihilation, including the effect of sink evolution resulting from defect annihilation.

The clustering, diffusion and ultimate annihilation of the vacancies, self-interstitials and point defect clusters occurs over timescales from nanoseconds to well in excess of seconds, as discussed in the preceding paragraphs, and alters the local chemistry and internal structure at the nanometer and micron length scale. Solutes and impurities are re-distributed as a consequence of radiation enhanced diffusion and radiation induced segregation processes, and the evolving local chemical environment will also influence the defect transport kinetics and mechanisms through a

variety of trapping interactions. Notably, while many of these interactions have been postulated, the atomistic interaction mechanisms remain to be quantified through modeling and focused experimental studies. Changes in nano/microstructure defect structure and local chemical arrangements are known to be responsible for dimensional instabilities, such as swelling and irradiation creep, and mechanical property degradation, including irradiation hardening, decreased work hardening, increased susceptibility to creep rupture and localized deformation, which impact component performance, reliability and ultimately, lifetime.

For example, it is well established that the effect of irradiation on ferritic/martensitic alloys at low to intermediate temperatures ($T < \approx 550$ °C) is to increase yield stress, reduce strain hardening capacity and initiate flow localization at lower strains [1-5, 24-34]. The predominant microstructural features observed in TEM studies are very small (~nm) cluster-type features, which may include dislocation loops, cavities and regions of solute segregation, as well as second phase precipitates [25-34]. The balance of these features depends on the synergistic interaction of key irradiation, material and environmental variables, including irradiation temperature, dose and dose rate, helium production and alloy composition. And thus, a comprehensive model that predicts the radiation damaged microstructures, with a quantitative assessment of the mix of features formed based on the key irradiation and metallurgical variables and indeed, the detailed mechanisms of their formation, as well as their precise character and composition, remain outstanding questions. The remainder of this article will describe the use of cluster dynamics and object kinetic Monte Carlo models, informed within a multiscale modeling methodology and closely coupled to experimental characterization of radiation-damaged body-centered cubic materials, which have successfully predicted the defect microstructure evolution in molybdenum, iron and iron-chrome based ferritic-martensitic alloys. These results will be

presented in Section 3, along with a discussion of the key assumptions inherent in the mean-field reaction-diffusion based cluster dynamics models, as well as the object kinetic Monte Carlo studies used to verify the mean field model. Section 4 will highlight a number of areas for future research needs that can be addressed using high-resolution characterization techniques, closely coordinated with modeling studies, before the article summarizes in Section 5.

2. MULTISCALE MODELING APPROACH APPLIED TO RADIATION DAMAGE

Figure 1b shows a schematic illustration of a science-based, and integrated experimental and computational modeling approach to investigating materials degradation in the fusion environment, within an information passing methodology. Akin to the multiscale materials processes controlling property degradation, illustrated in Figure 1a, a multiscale approach is required to determine the controlling mechanisms and processes. Figure 1b illustrates the hierarchical multiscale modeling methodology, which integrates *ab initio* electronic structure calculations, molecular dynamics (MD) simulations, kinetic Monte Carlo (KMC), rate theory simulations with thermodynamics and kinetics through the passing of information about the controlling physical mechanisms over the relevant length and time scales to model the fates of defects and solutes during high-energy neutron irradiation and thus, predict nano/microstructural evolution. Detailed microstructural information can then used as a basis for modeling the mechanical behavior through meso (represented by 3D dislocation dynamics) and continuum scale models, which must be incorporated into fracture mechanics models at the continuum scale in order to predict material deformation and failure of individual reactor components, and which would provide predictive materials performance models for integrated system evaluation through finite element modeling. In this figure, individual modeling techniques are identified in a series

of linked process ellipses, with representative schematics illustrating the type of modeled material behavior through the length and timescales. The passing of information between the scales is represented through a series of arrows. Of course, multiscale modeling by itself is insufficient to fully predict the performance of complicated engineered structures in the fusion environment, and the science-based multiscale paradigm involves a close integration with a suite of experimental characterization techniques. A sub-set of these techniques is represented for microstructural characterization on the lower side of the gray sphere and for experimental mechanical behavior/testing methods on the upper side.

Due to space limitations, in this article we will focus entirely on the microstructural (or mesoscale) modeling of defect cluster evolution in irradiated materials using mean field reaction-diffusion cluster dynamics models, which are an extension of the classical rate theory model of radiation damage, and with cross-comparison for model verification through the use of object kinetic Monte Carlo simulations. This region of the multiscale materials modeling paradigm shown in Figure 1b has therefore been highlighted with an orange ellipse. In the remainder of this section, we do not fully describe the range of models illustrated within Figure 2, but rather we will focus on a succinct description of the cluster dynamics and kinetic Monte Carlo models that are the focus of the work described here.

Cluster dynamics model based on reaction-diffusion rate theory

Isolated vacancies and self-interstitial atoms (SIAs), as well as three-dimensional vacancy clusters and clusters of SIA in the form of planar, prismatic dislocation loops are continuously formed and will evolve in pure body-centered cubic iron under neutron irradiation [9-11, 35-37]. A cluster dynamics (CD) model based on the reaction-diffusion rate theory is used here to

predict the evolution of the vacancy and SIA defect clusters, which is a modified version of the model developed by Xu and Wirth [35, 38-40] and only considers the intrinsic defects and their clusters. Furthermore, since the probability that SIA and vacancy co-exist in a single cluster is very low due to their strong tendency for recombination, no mixed I-V clusters are considered, and it is thus sufficient to define any cluster using just an integer, with its absolute value being the number of point defects contained in the complexes and its sign ('−' for SIA clusters, or '+' for V-clusters) indicating the character of the cluster. Two numbers, NI and NV, are chosen as the number of interstitials in the largest SIA-cluster, and the number of vacancies in the largest V-cluster, respectively. Physically, these numbers prescribe the 'phase space' within which the clusters can interact with each other, and ensure the conservation of point defects. NI and NV should be chosen sufficiently large so that the computational results are not impacted by a prescribed phase space that is too small (e.g., insufficient cluster size to allow growth to large defect cluster size).

For neutron irradiation, it is common to model the system without a discrete spatial dependence, making use of the mean field approximation, as described here. However, for many cases of ion irradiation, and in particular for thin-film ion irradiation studies, the spatial dependence of the damage profile, and the strong influence of the free surfaces, requires an explicit spatial dependence in the model developed by Xu and Wirth [35, 38-41]. As well, the nature of defect generation in metals induced by ions and neutrons is significantly different. The energy transfer cross section for ion – atom collisions is an atomic cross section (~ 10^{-17} cm^2) while that for neutrons is a nuclear cross section (~10^{-24} cm^2), and consequently, neutrons have a much larger range between collisions when travelling in a material. The damage production varies weakly

along the depth direction for neutron irradiation and therefore, it is reasonable to treat the distribution of radiation damage production as homogeneous [43, 44, 45]. Thus, as noted previously, no explicit spatial dimension is necessary in this model, at least for low neutron dose levels before a clear spatial correlation of the defect microstructure develops.

Without an explicit spatial dependence, the concentration of each cluster is only a function of time, and ordinary differential equations describe the defect evolution. The binary reactions discussed in Refs. [35-41] are still appropriate and become simpler, because there are only two types of defects (V- and SIA-clusters) considered during neutron irradiation. The generic form to describe the evolution of a cluster, without spatial dependence, is:

$$\frac{dC_i}{dt} = \phi \times P_i + G\_T + G\_E - A\_T - A\_E \,, \tag{1}$$

where C_i refers to the volumetric concentration (in 1/m^3) of the i-th cluster, ϕ is the neutron flux (in neutron/m^2/sec), P_i is the production 'probability' of the i-th cluster by neutron irradiation, G refers to the collective generation rates, where G_T refers to generation by trapping and G_E refers to generation by emission, A_T indicates the annihilation of cluster C_i by trapping events, and A_E refers to annihilation by emission events. The detailed construction of the coupled system of ODEs is thus (for which $\Lambda = \left[-NI, NV\right]$ is the prescribed phase space):

$$\frac{dC_i}{dt} = \phi \times P_i + \sum_{\substack{m+p=i \\ m,p\neq 0 \\ m.p\in\Lambda}} k^+_{m,p} C_m C_P - \sum_{\substack{m\neq i \\ m\neq 0 \\ m.m+i\in\Lambda}} k^+_{m,i} C_m C_i - k^-_i C_i \tag{2}$$

for i=NV or –NI, and

$$\frac{dC_i}{dt} = \phi \times P_i + \sum_{\substack{m+p=i \\ m,p\neq 0 \\ m.p\in\Lambda}} k^+_{m,p} C_m C_P + k^-_{i+1} C_{i+1} - \sum_{\substack{m\neq i \\ m\neq 0 \\ m.m+i\in\Lambda}} k^+_{m,i} C_m C_i - k^-_i C_i \qquad (3)$$

for $\frac{NV}{2} < i < NV$, and

$$\frac{dC_i}{dt} = \phi \times P_i + \sum_{\substack{m+p=i \\ m,p\neq 0 \\ m.p\in\Lambda}} k^+_{m,p} C_m C_P + k^-_{i+1} C_{i+1} - \sum_{\substack{m\neq i \\ m\neq 0 \\ m.m+i\in\Lambda}} k^+_{m,i} C_m C_i - 2k^+_{i,i}\left(C_i\right)^2 - k^-_i C_i \qquad (4)$$

for $2 \le i \le \frac{NV}{2}$, and

$$\frac{dC_i}{dt} = \phi \times P_i + \sum_{\substack{m+p=i \\ m,p\neq 0 \\ m.p\in\Lambda}} k^+_{m,p} C_m C_P + 2k^-_2 C_2 + \sum_{\substack{m>2 \\ m\in\Lambda}} k^-_m C_m - \sum_{\substack{m\neq i \\ m\neq 0 \\ m.m+i\in\Lambda}} k^+_{m,i} C_m C_i - 2k^+_{i,i}\left(C_i\right)^2 \qquad (5)$$

for $i = 1$, and

$$\frac{dC_i}{dt} = \phi \times P_i + \sum_{\substack{m+p=i \\ m,p\neq 0 \\ m.p\in\Lambda}} k^+_{m,p} C_m C_P + 2k^-_{-2} C_{-2} + \sum_{\substack{m<-2 \\ m\in\Lambda}} k^-_m C_m - \sum_{\substack{m\neq i \\ m\neq 0 \\ m.m+i\in\Lambda}} k^+_{m,i} C_m C_i - 2k^+_{i,i}\left(C_i\right)^2 \qquad (6)$$

for $i = -1$, and

$$\frac{dC_i}{dt} = \phi \times P_i + \sum_{\substack{m+p=i \\ m,p\neq 0 \\ m.p\in\Lambda}} k^+_{m,p} C_m C_P + k^-_{i-1} C_{i-1} - \sum_{\substack{m\neq i \\ m\neq 0 \\ m.m+i\in\Lambda}} k^+_{m,i} C_m C_i - 2k^+_{i,i}\left(C_i\right)^2 - k^-_i C_i \qquad (7)$$

for $-\frac{NI}{2} \le i \le -2$, and

$$\frac{dC_i}{dt} = \phi \times P_i + \sum_{\substack{m+p=i \\ m,p\neq 0 \\ m.p\in\Lambda}} k^+_{m,p} C_m C_P + k^-_{i-1} C_{i-1} - \sum_{\substack{m\neq i \\ m\neq 0 \\ m.m+i\in\Lambda}} k^+_{m,i} C_m C_i - k^-_i C_i \qquad (8)$$

for $-NI < i < -\frac{NI}{2}$, where k^+ is the forward reaction rate constant and k^- is the backward reaction rate constant, having the same expressions as the classic rate theory derviations based on isotropic interactions and spherical reaction volumes as derived by Waite based on the original work of Smoluchowski [42,43], i.e.,

$$k^+_{m.p} = 4\pi(r_m + r_p)(D_m + D_p), \qquad (9)$$

$$k^- = k^+ C_0 \exp\left(-\frac{E_b}{k_B T}\right), \qquad (10)$$

where r_m and r_p are the trapping radii of clusters m and p, D is the diffusion coefficient of the reacting species, C_0 is the atomic number density of the iron matrix, E_b is the binding energy of a single point defect to the cluster, k_B is Boltzmann's constant, and T is the temperature. Note that for emission ($C \rightarrow A + B$), only those events in which at least one of the two products is a monomer (i.e., I or V) are considered since it is in general more energetically favorable for a cluster to emit a monomer than emit a dimer, trimer or larger cluster, which is consistent with previous models [38-40].

The variations among equations (2)-(8) represent the computational details in the cluster dynamics modeling, which must be considered to ensure no computational artifacts (such as non-conservation of point defects) are introduced in the results. For example, the difference between Eq. (7) and (8) is that in Eq. (7) the interstitial clusters, I_n, where n is less than half of the pre-set maximum interstitial clusters size, are allowed to interact with similar sized clusters to generate a big cluster. However, in Eq. (7), this behavior is forbidden due to the fact that the resulting larger interstitial cluster would exceed the prescribed phase space. If we were able to solve an infinite number of equations/clusters in computation, this would not be necessary, but in reality, we can only solve finite, although fairly large, number of coupled equations and hence these detailed rules of computation have to be enforced.

Object kinetic Monte Carlo model

A different computational approach, namely, object kinetic Monte Carlo (OKMC), has also been used to simulate 1 MeV Kr^+ ion irradiation in thin molybdenum foils, and to compare with both the spatially-dependent version of the cluster dynamics model as well as in-situ TEM

experiments. OKMC tracks the 3-D spatial position of each individual defect cluster ("object") from birth until annihilation. A cluster can be "born" through direct cascade creation, reactions between two clusters, or one parent cluster undergoing thermal emission. A cluster can be "annihilated" by the cluster changing its size as a result of capturing another cluster or thermally emitting a monomer, or jumping to free surface sink. Further, a cluster can change its position as a result of diffusive jumps. While atomistic mechanisms of diffusion and cluster reaction are considered in rate theory models, an OKMC model explicitly tracks the three-dimensional position and identity of individual defect clusters rather than imposing a *mean field* concentration/density and is thus not subject to the limiting assumptions of rate theory. In radiation damage research, OKMC has often been used to validate sink strength or rate constant formulations that are required by rate theory or CD models [44-46] in the regime where their basic assumptions stand, but the use of OKMC to follow an entire irradiation process independently has been rare due to relatively high computational cost [47]. Xu and Wirth have recently developed an OKMC code that uses a "cell" algorithm to significantly reduce unnecessary iterations in the judgment of capturing of a cluster by any other cluster [48]. The new algorithm, combined with adaptive OpenMP parallelism, allows a fairly large simulation box with a volume of 6×10^{7} nm^3 which corresponds to a minimum resolvable defect density of 1.67×10^{-8} nm^{-3} (for one defect in the box).

Black-sink boundary conditions, in which all defect concentrations are set equal to zero, are enforced along one dimension of the rectangular simulation box that represents the foil depth (36, 60, 84, 110 nm), while periodic boundary conditions are applied along the other two dimensions. Small interstitial (I) and vacancy (V) clusters, with sizes in the range from I_1~I_{20} and V_1~V_9, are created randomly in the simulation box at frequencies $\nu_{C,i} = V_{box}\phi P_i$, where V_{box} is the

volume of the simulation box in nm^3, ϕ is the ion flux in ion/(nm^2 sec) and P_i is the production probability of the cluster *i* in 1/(ion nm) determined through MD (molecular dynamics) cascade simulations [10] and SRIM recoil energy calculations [49], as described in more detail in Ref [48]. An already existing cluster can migrate by taking random jumps at a frequency $\nu_{J,i} = \nu_{0,i} \exp\left[-E_{m,i} / \left(k_B T\right)\right]$, where $\nu_{0,i}$ is the attempt frequency and $E_{m,i}$ is the migration energy of the cluster *i*. The attempt frequency is related to the diffusivity pre-factor D_0 as $\nu_0 = 2n \times D_0 / l^2$, where *l* is the jump distance (taken as the nearest neighbor distance) and *n* is a dimensionality number (e.g., n=3 for 3-D diffusion). Diffusivity pre-factors and migration energies of the interstitial clusters and single vacancy are provided in Table 1, with more detail provided in Ref. [35]. Note that these mobility data have been optimized based on an *effective* 3-D diffusion mode that provides a simple but sufficient representation of mixed 1-D migration and rotation for interstitial loops. For the purpose of comparing with the CD model, the effective 3-D diffusion mode is retained in this present OKMC study, although it will be interesting in the future to implement mixed 1-D migration and rotation directly. Further, an existing cluster *i* can also emit monomers (single interstitials or single vacancies) by thermal activation at a frequency $\nu_{E,i}$ co-determined by diffusivities and the binding energy. For example, the frequency of a V_n cluster emitting a single vacancy is $4\pi\left(R_{V_1} + R_{V_{n-1}}\right)\left(D_{V_1} + D_{V_{n-1}}\right)\exp\left[-E_{b,V_n} / \left(k_B T\right)\right] / \Omega$ where *R* is the cluster radius, Ω is the atomic volume, and E_{b,V_n} is the binding energy. The binding energy values have been obtained by extrapolating from ab initio calculated monomer formation energy (E_{f,V_1}) and di-vacancy binding energy (E_{b,V_2})[50] through a well-accepted 2/3-power law: $E_{f,V_1} + \left(E_{b,V_2} - E_{f,V_1}\right)\left[n^{2/3} - \left(n-1\right)^{2/3}\right] / \left(2^{2/3} - 1\right)$ [14]. It should be noted that another expression

existing in the literature for calculating the emission frequency, namely, $\nu_{J,V_1} \exp\left[-E_{b,V_n} / \left(k_B T\right)\right]$, is not entirely appropriate for OKMC since it fails to consider all the monomers on a cluster surface attempting to break away, although it is correct for atomistic KMC. Based on the frequencies, a single event is selected at each OKMC step out of all the time-requiring events (creation/jumping/emission) and the time is incremented using the well-known residence-time algorithm (see, e.g., [51]). Upon each event, the code checks for possible trapping, surface annihilation and/or translation across periodic boundaries, which are considered to occur instantaneously.

3. RESULTS OF DEFECT CLUSTER EVOLUTION IN IRRADIATED BCC MATERIALS

1 MeV Kr irradiation of Mo in the IVEM

Xu and Wirth, working closely in parallel with the experimental investigation by Li and Kirk, have focused on developing and validating the spatially-dependent reaction diffusion cluster dynamics (CD) model for 1 MeV Kr^+ irradiation in thin molybdenum (Mo) foils at 80°C [35,48,52,53]. Fluxes of 1.6×10^9, 1.6×10^{10} and 1.6×10^{11} ions/cm^2/s were used and fluences of up to 5×10^{12} ions/cm^2 were reached. A large amount of data was obtained by Li and Kirk [53] in the in-situ TEM experiments based on continuous visualization of the defect evolution from the start of the irradiation. Specifically, the defect density and sizes were obtained at many different doses (fluences) and foil thicknesses (~10 to ~100 nm) at all three fluxes. The observed defects were

confirmed to be dislocation loops with an average of ~77% possessing a Burgers vector of ½<111> and ~23% possessing <100>.

While not shown here, the CD model, which was parameterized based on the use of radiation damage produced in the form of only single vacancy and self-interstitials as isolated Frenkel pairs, predicted visible defect cluster areal densities that were many of orders of magnitude below the experimentally observed values that were in the range of $0.2\text{-}5\text{x}10^{-3}$ nm^{-2} [35]. Likewise, with the assumption of spherical, isotropic reaction rate constants that follow the Smoluchowski definition in Eq. (9), it was not possible to obtain good agreement between the model predictions and the experimental results of areal defect cluster density and the observed defect cluster size distribution if the only mobile species were single vacancies and single self-interstitial atoms, even including the direct formation of interstitial clusters within the displacement cascade [35]. Good agreement was obtained, as shown in Figure 2, across a range of thin foil thickness and ion flux and fluence values for 1 MeV Kr ion irradiation at a temperature of 80°C, when incorporating defect production due to displacement cascade formation and the possible mobility of a large number of interstitial cluster defects.

However, a key uncertainty in the model was how best to parameterize the mobility of self-interstitial clusters. Molecular dynamics simulations have revealed both the formation of crowdion clusters in displacement cascades [9-11], as well as the very high mobility of these clusters [14-16], which can also be thought of as prismatic dislocation loop embryo, in one-dimension along their Burgers vector. These MD observations led to the idea of the production bias model extension of the classical rate theory [54], but experimental observations in the TEM by Arakawa and co-workers [55] have indicated that the loop migration energies are much higher than observed in the MD simulations. Arakawa further postulated that the higher activation

energies for loop migration were due to the strain field interactions between the prismatic dislocation loops and interstitial type impurities within the matrix, akin to Cottrell atmosphere interactions responsible for Luders band behavior [56]. Thus, the activation energy for interstitial cluster and small interstitial cluster diffusion was treated as a fitting parameter in this work, utilizing only a sub-set of the experimental data. The resulting optimized interstitial cluster diffusion coefficients are presented in Table 1, and the strikingly good agreement between the experimental and model predictions across two orders of magnitude of ion flux (which were not included in the parameter optimization) provide a validation of the CD model and approach, at least for irradiation temperatures around 80°C.

Xu and co-workers also verified this CD model by comparing to OKMC simulations, as described in more detail in Ref [48]. Figure 3 compares the areal density of visible defects as a function of ion fluence obtained from OKMC and our previous spatially-dependent cluster dynamics model for three foil thicknesses (36, 60, 84 nm) at three ion fluxes: 1.6×10^{11} (a), 1.6×10^{10} (b), and 1.6×10^{9} (c) ions cm^{-2} s^{-1}. Clearly, the OKMC and the CD not only predict the same qualitative trend of increasing areal density with increasing ion fluence, foil thickness and ion flux, but they are also in excellent quantitative agreement such that the two sets of data nearly completely overlap. While not shown here, the two computational approaches also predict essentially identical size distributions of the visible defect clusters. The strong agreement between the OKMC and the CD results confirms, within the scope of the effective 3-D diffusion mode, the numerical fidelity of the extended CD model for the study of the defect agglomeration in the thin foils, even though some non-conventional aspects have been utilized in the CD model, namely, the separated inter-grid diffusion and intra-grid reaction, the large number of different sized mobile clusters, the extremely small (nanometer scale) sample thickness and spatial

meshes, and the fixed surface sink positions. The effect of these assumptions, along with challenges to extend this model to higher radiation dose levels, will be discussed in Section 4.

Neutron irradiation of Fe

Hu and co-workers [41] modeled the neutron irradiation of nominally pure iron within the temperature range of 60 to 100°C, and compared the model predictions of black dot defect density to TEM observations, and vacancy size distribution to positron annihilation measurements. Table 2 presents the kinetic parameterization of vacancy and self-interstitial atom cluster diffusivity used for iron, which was based on a similar approach to that used by Xu and co-workers for molybdenum. Figure 4 presents modeling results of the vacancy and interstitial cluster distributions as a function of irradiation dose. It can be seen that interstitials undergo significant clustering at these doses and temperatures, while vacancies do not. This reflects the fact that interstitials are much more mobile than vacancies. By comparing Fig. 4(a) and 4(b), one can see that clustering of both interstitials and vacancies is larger at the slightly higher temperature at 100°C.

Eldrup et al. [57] used PAS to obtain information on the vacancy cluster populations in pure iron after these same neutron irradiation conditions. In the quantitative analysis, the measured lifetime spectra for the irradiated Fe samples were resolved into five lifetime components, four of which have fixed lifetimes: 200, 300, 400, and 500 ps, equivalent to three dimensional vacancy clusters with a size of about 0.35, 0.54, 0.73, and > 1.0 nm in diameter, respectively. The application of the trapping model to the measured positron lifetime spectra was used to obtain the density of different defect clusters, providing a rough size distribution of

vacancy clusters in iron under various irradiation conditions, shown in Figure 5. The output from the CD model predictions, similar to that shown in Fig. 4 but at an appropriate dose level, can be easily analyzed to extract the quantities that are acquired in the experiments so that direct comparisons can be drawn between the modeling predictions and the PAS measurement. For example, the total volumetric density of vacancy clusters can be obtained by summing over different defects, and the size distribution can be obtained by binning the defects into various size intervals and summing the volumetric densities within each bin. In Fig. 5, the modeling results of the vacancy cluster size distributions at 60° and 100°C are plotted together with the PAS measurements for three different irradiation doses of 0.0001, 0.0009 and 0.009 dpa. Generally, the modeling results show a similar trend of increasing density of increasing cluster sizes with increasing radiation dose, as the experimental measurements. For the neutron irradiation doses of 0.0001 dpa and 0.0009 dpa, the PAS experimental analysis indicates that most of the vacancy clusters have a size less than 3.5 nm and the densities decrease with increasing sizes. The models reproduce these features except the modeling predictions at 0.0009 dpa at 100°C, for which the vacancy clusters of intermediate sizes have a slightly larger volumetric density. When the neutron dose increases to 0.009 dpa, the PAS results show that the vacancy clusters with diameters in a range of 0.35-0.54 nm are dominant in the measured positron lifetime spectra, which is also in good agreement with the model predictions. Overall, the modeling predictions at these two temperatures bracket the PAS measurements, and are in quite good agreement when considering the uncertainty within the experimental measurements.

The PAS thus provide a comparison and verification of the vacancy cluster distribution predicted by the cluster dynamics model based on reaction-diffusion rate theory. As well, it is important to validate the modeling prediction of the interstitial cluster distribution. Ref. [57]

describes the results of a TEM investigation on the neutron irradiated Fe samples performed to characterize the density of the interstitial type dislocation loops. It is important to note that not all interstitial clusters, but only those with a diameter exceeding the TEM resolution limit, can be observed by TEM. Further, not all dislocation loops will be resolvable in the TEM due to the $\boldsymbol{g \cdot b}$ invisibility criteria [53]. The resolution limit in such TEM experiments varies slightly with material condition as well as TEM operating conditions, but is generally in the range of 1.0-1.6 nm. In BCC iron, a 1.4 nm diameter corresponds to a 32-member interstitial cluster (I_{32}) of 2-D planar shape, and a 1.6 nm diameter corresponds to I_{42}. This implies that the comparison of the modeling results and the experimental observations will be sensitive to the choice of the TEM resolution limit. Figure 6 shows the TEM observations (in blue squares) and the modeling results at the neutron irradiation temperatures of 60 and 100°C for four different TEM resolution limits. The simulation results are always higher than experimental data. This discrepancy could be ascribed to both modeling predictions and experimental observations. For the mean-field reaction-diffusion cluster dynamics model, the introduction of new clusters by neutron irradiation is independent of the existing clusters. However, MD simulations indicate the possible reaction amongst pre-existing defect clusters and a newly produced displacement cascade, which can result in, additional recombination or clustering reactions that limits nucleation of new defect clusters. However, the MD database and understanding of the way in which these reactions occur is currently insufficient to appropriately model the reaction rate density, and thus, this effect is not included in the current model, which may result in a slight overestimation of defect clusters. On the other hand, not all interstitial clusters are resolvable in TEM observations due to the $\boldsymbol{g \bullet b}$ invisibility criteria [53]. This possible underestimation may also contribute to the discrepancy between the modeling and experimental results.

Although there are some quantitative differences between the modeling and TEM measurements, the order of the magnitude of the interstitial cluster densities are generally comparable, and within the experimental error usually estimated to be about an order of magnitude [57]. It is noted that the lower the TEM resolution limit (larger diameter for the smallest observable loop), the better the agreement between the experimental measurements and the modeling. Also, the modeling predictions at 100°C agree slightly better with the experimental observations than the lower temperature of 60°C. Another important parameter for the validation of the developed model is the average dislocation loop size, which is obtained from weighted average of visible interstitial clusters. The comparison between modeling predictions and experimental observations [58] of visible loop size is shown in Fig. 6b, and demonstrates that a quite good agreement is achieved, especially for the higher two doses and higher temperature model predictions. Overall, the agreement observed for both the vacancy and interstitial cluster size distributions for the case of neutron irradiated iron again gives confidence in the CD modeling approach and assumptions, and Section 4 will discuss some outstanding questions that remain to be addressed.

1 MeV Kr irradiation of Fe-Cr ferritic/martensitic alloys in the IVEM

A wide variety of detailed data on the development of intermediate dose (less than ten dpa) irradiation damage microstructures in ferritic/martensitic steels and other bcc alloys has been produced by in situ ion irradiation studies [59-65]. Such experiments allow irradiation concurrent with observation in a transmission electron microscope. A black dot damage microstructure is seen to dominate irradiated ferritic/martensitic alloys up to temperatures of at least 300°C [59-63,66,67]. At higher temperatures, extended prismatic dislocation loops with

a/2<111> or a <100> Burgers vectors are clearly distinguished. Notably, as shown in Figure 7, there is relatively little temperature dependence on the saturation number density in either model Fe-Cr based ferritic-martensitic alloys studied by Kaoumi and co-workers [63] or in the commercial alloy NF616 studied by Topbasi and Motta [62,67].

The black dots which form at lower temperatures are presumably also interstitial type loops of a sufficiently small size that the dislocation itself cannot be resolved. These two to five nm features become difficult to analyze because of their size, however, limiting confident assessments of type or Burgers vector. Numerous studies have indicated that these features grow in density up to a saturation value past which any further evolution is restricted to the defect size [62,63]. In-situ experiments have provided new clues as to the properties of these defects. Under both electron and heavy ion irradiation, the thermally immobile damage features have been widely observed to undergo occasional but rapid translations spanning distances on the order of a few to a few tens of nanometers which punctuate extended periods where no motion occurs at all [60,67-70]. Notably, these “hops" generally occur only when the ion or electron beam is operating and occur over the entire regime of black dot damage, even at temperatures as low as 50 K. The limited mobility of such features contrasts vividly with predictions about their motion based on molecular dynamics simulations, in which interstitial clusters diffuse along one dimensional trajectories with very low (less than 0.1 eV) activation energies [14-16]. The reconciliation of disparate expected and observed behaviors has been rationalized by “traps", broadly defined as a variety of impurities or impurity defect complexes which bind to the dislocation loops and lower their mobility. Though multiple candidates for the composition of such traps have been proposed, trapping has been invoked to explain the lower than expected thermal mobility of loops [14] as well as the hops seen in irradiation environments [68,69].

Kohnert [71,72] has included a beam-assisted mobility to account for the aforementioned "hops" of black dot defects during the in-situ ion irradiations, by modeling the diffusivity of interstitial clusters within the cluster dynamics framework described in Eqs (1-10), as:

$$D = D_o e^{-E_m/kT} + \frac{\lambda_{irr}}{2N}\nu_{irr} \quad (11),$$

where the first term describes the normal Arrhenius type diffusion, and the second term describes the dynamic behavior observed during in situ experiments where thermally immobile (presumably trapped) loops undergo occasional but rapid translations. Presumably this erratic motion during the ion irradiation is due to a series of ballistic de-trapping events induced by energetic recoils. The effective diffusivity due to such ballistic motion is described with an activation frequency, ν_{irr}, and a discrete hop length, λ_{irr}, which describes the effective distance between hops, and where N is the dimensionality of diffusion (assumed to be three-dimensional based on observed erratic nature of the motion).

Figure 8 demonstrates the CD model predictions for 1 MeV Kr ion irradiation of ferritic-martensitic alloys, as compared to the saturation density observed by Kaoumi et al. [63], and Topbasi et al. [62,67]. Here the thermal diffusion of large interstitial clusters are based on an activation energy of 1.3 eV, consistent with in situ TEM observations of Arakawa [55], as discussed earlier. The activation energies for the single interstitial and small interstitial clusters are set equal to values obtained from ab initio calculations [73,74], while all interstitial clusters greater than size 3 are set to the saturation value. There are subtle differences between Model I and II in terms of the activation energy of the single vacancy and small vacancy clusters, wherein Model I uses a value of 1.3 eV for v1, v2, v3 and v4, whereas Model II sets the migration energy for the single to quad-vacancy cluster to the values from ab-initio calculations, which range from

0.35 (v3) to 0.67 (v1) eV [73]. Notably, when the beam-assisted diffusion term, Eq. (11), was not included, the predicted areal defect density did not saturate but experiences breakaway growth. As shown in Figure 8, both model I and II predict a temperature dependence of the defect cluster saturation density that is consistent with the experimental observations. This can be rationalized due to the nucleation and growth behavior of the defect cluster density, and the fact that the beam assisted diffusivity provides a mechanism for cluster sizes which would otherwise be thermally immobile to interact with each other.

4. DISCUSSION OF OUTSTANDING ISSUES

In this report, we have provided a review of three recent modeling studies that have compared reaction-diffusion based cluster dynamics models to in-situ TEM studies of the defect accumulation during 1 MeV Kr ion irradiation of nominally pure molybdenum or ferritic-martensitic steels, in addition to neutron irradiation of nominally pure iron. Overall, the agreement between the modeling predictions and the experiments is quite good, and demonstrates an impressive ability to capture the multiscale nature of radiation effects on structural materials, at least in terms of the evolution of the interstitial defect clusters which develop into the black dot structure of prismatic dislocation loops in bcc materials at intermediate radiation temperature, as well as the sub-visible vacancy cluster distribution in neutron irradiated iron. Indeed, the in situ TEM irradiation experiments provide a unique opportunity to examine the fine details of defect evolution under continuous irradiation, and, when combined with cluster dynamics modeling, provide a nice opportunity to verify fundamental assumptions/uncertainties with respect to damage production and kinetics/energetics of irradiation defects.

While the results presented here do provide a good agreement with the experimental observations, there are a number of assumptions inherent in these modeling results, which merit further investigation. First and foremost is the assumption of the isotropic three-dimensional reaction kinetics that underpin the Smoluchowski reaction rate constants of Eq. (9). Kohnert has begun to investigate this assumption in detail, as have Barashev and co-workers [75]. However, the mathematical formulations rapidly become quite complex within models that have multiple diffusing species, as is necessary to treat the prismatic interstitial loop behavior in real-world materials containing impurities, and for which the resulting migration behavior is presumably determined trapping and de-trapping interactions. While the effective isotropic diffusion assumed within the modeling results presented from Xu on the defect cluster evolution in molybdenum [35,48,52-53] and Hu for the neutron irradiation results in iron [41] are quite impressive, clearly these models need to be validated by comparison to experimental data across a much wider temperature regime. Thus, there is a need for additional, high-fidelity experimental characterization of the defect cluster microstructure in irradiated materials with irradiation temperatures ranging from below Stage III to near Stage V in order to validate the defect cluster diffusion kinetics and reaction rate constants that are inherent to the reaction-diffusion cluster dynamics, or object kinetic Monte Carlo modeling approaches.

Another import aspect of the visible defect cluster evolution is the identity of the Burgers vector of the visible loop populations. It is well established that in iron and other bcc materials, that some portion of the prismatic loop population following irradiation has Burgers vector of a<100>, and in some cases, the fraction of <100> loops is dominant. In the modeling presented here, no discrimination has been made between possible a/2<111> or a<100> dislocation loops since this would require parameterization of cluster type to evaluate the multiple models that

have been proposed in the literature to explain the a<100> loop formation. However, this is a topic which the models should be able to address in the near future, especially given the continual increases in computational capability and memory required to treat ever larger reaction networks. Such modeling efforts would be further complemented by additional detailed microscopy to expand the database of loop populations as a function of irradiation conditions and the type of bcc material.

The results presented here are also limited to rather small radiation damage levels below a few displacements per atom. As noted by Li and co-workers in describing the experimental observations in Mo [53], and by Kaoumi and co-workers in the ferritic-martensitic alloys [63], at higher doses, a pronounced rafting or spatial arrangement was observed in the visible defect cluster distributions. This has not been captured within the current models, which are limited to one spatial dimension, and for which elastic interactions amongst the defect clusters and other microstructural features are not included. But, clearly, this is another need for coordinated modeling and experimental studies in the future. It can be further supposed that the observed dislocation loop rafting behavior may be responsible for the saturation of the mechanical properties that is observed at higher doses in structural materials. Unraveling this will require a combination of spatially resolved, e.g., tomographic, studies of the evolution of the defect cluster distributions across a range of radiation exposures and temperatures, coordinated with extensions of the multiscale modeling methodology to specifically investigate the role of elastic interactions amongst defect populations to describe such higher dose behavior.

Finally, the modeling results here have focused entirely on the evolution of vacancy and interstitial type defect clusters in irradiated bcc materials, without any consideration of the coupling of the defect and solute/impurity fluxes. There is a long-standing literature on the

radiation induced segregation in austenitic alloys, as well as more recent work on radiation-induced segregation in ferritic-martensitic materials. This article has not attempted to review that literature, other than to note that this is an area which is receiving increasing attention towards coupling the defect and solute fluxes which occur under irradiation to thermodynamic predictions of radiation-induced phase formation.

5. SUMMARY

As highlighted here, cluster dynamics (CD) models provide a powerful reaction-diffusion rate theory based modeling approach that allow high fidelity calculations of the density of irradiation induced defects and their contributions to long term microstructural evolution. This article has reviewed three recent applications of CD models, including the verification of the computational fidelity of the model against object kinetic Monte Carlo models, which predict the visible defect cluster distributions that evolve in molybdenum, iron and ferritic-martensitic alloys up to radiation dose levels on the order of a few displacements per atom. We have also identified several areas that require further coordinated experimental characterization and modeling, including the diffusivity and reaction kinetics of small interstitial clusters in bcc materials, the evaluation of the multiple models to rationalize the formation of prismatic loops with a<100> Burgers vectors in irradiated bcc materials, and the formation of spatial arrangements, or rafts, of dislocation loops which is observed at higher radiation doses.

7. REFERENCES

1. G. R. Odette, B. D. Wirth, D. J. Bacon and N. M. Ghoneim, *MRS Bulletin*, **26** (2001) 176.
2. E.E. Bloom, *J. Nucl. Mat.*, **258-263** (1998) 7.

3. E. E. Bloom, N. Ghoneim, R. Jone, R. Kurtz, G. R. Odette, A. Rowecliffe, D. Smith and F. W. Wiffen, "Advanced Materials Program", appendix D of the VLT roadmap, 1999, available at http://vlt.ucsd.edu/.
4. S.J. Zinkle and N.M. Ghoniem, *Fusion Engineering & Design* **51-52** (2000) 55.
5. T. Muroga, M. Gasparotto, and S.J. Zinkle, *Fusion Engineering & Design* **61-62** (2002) 13.
6. M. Victoria, N. Baluc, C. Bailat, Y. Dai, M.I. Luppo, R. Schaublin, and B.N. Singh, *J. Nuclear Materials* **276** (2000) 114-122.
7. T. Diaz de la Rubia, H.M. Zbib, T.A. Khraishi, B.D. Wirth, M. Victoria and M.J. Caturla, *Nature* **406** (2000) 871.
8. B.D. Wirth, G.R. Odette, J. Marian, L. Ventelon, J.A. Young and L.A. Zepeda-Ruiz, *Journal of Nuclear Materials* **329-333** (2004) 103.
9. G.J. Ackland, D.J. Bacon and A.F. Calder, *Phil Mag A* **75** (1997) 713.
10. R.E. Stoller, G.R. Odette and B.D. Wirth, *J Nucl Mat* **251** (1997) 49.
11. W.J. Phythian, R.E. Stoller, A.J.E. Foreman, A.F. Calder, and D.J. Bacon, *J. Nuc. Mat.* **223** (1995) 245.
12. J. B. Gibson, A. N. Goland, M. Milgram, and G. H. Vineyard, *Phys. Rev.* **120** (1960) 1229.
13. R.S. Averback and T. Diaz de la Rubia, *Solid State Physics*, **51** (1998) 281.
14. N. Soneda, and T. Diaz de la Rubia, Phil Mag A 78 (1998) 995.
15. B.D. Wirth, G.R. Odette, D. Maroudas and G.E. Lucas, *J. Nuc. Mat.,* **276** (1999) 33.
16. Y. N. Osetsky, M. Victoria, A. Serra, S. I. Golubov, and V. Priego, *J. Nucl. Mat.,* **251** (1997) 34.
17. B.D. Wirth, G.R. Odette and R.E. Stoller, *MRS Soc. Symp. Proc* **677** (2001) AA5.2.
18. H.L. Heinisch and B.N. Singh, *J. Nuc. Mat.*, **251** (1997) 77.
19. M.J. Caturla, N. Soneda, E.A. Alonso, B D. Wirth and T. Diaz de la Rubia, *J. Nuc. Mat.*, **276** (2000) 13.
20. P.R. Monasterio, B.D. Wirth and G.R. Odette, *J. Nucl. Mater* **361** (2007) 127.
21. G. Nandipati, W. Setyawan, H.L. Heinisch, K.J. Roche, R.J. Kurtz, and B.D. Wirth, *J. Nucl. Mater* (2014), doi: http://dx.doi.org/10.1016/j.nucmat.2014.09.067
22. M. Eldrup and B.N. Singh, *Mat. Sci. Forum* **363-365** (2001) 79.
23. B.D. Wirth, G.R. Odette, P. Asoka-Kumar, R.H. Howell, and P.A. Sterne, Proceedings of the 10th International Symposium on Environmental Degradation of Materials in Light Water Reactors, Ed., G.S. Was, National Association of Corrosion Engineers, 2002.
24. G. R. Odette, *J. Nuc. Mat*., **155-157** (1988) 921.
25. H. Matsui, K. Fukumoto, D. L. Smith, H. M. Chung, W. van Witzenburg, S. N. Votinov, *J. Nuc. Mat*., **233-237** (1996) 92.
26. R. Schaublin, P. Spatig and M. Victoria, *J. Nuc. Mat*., **258-263** (1998) 1178.
27. A. F. Rowcliffe, J. P. Robertson, R. L. Klueh, K. Shiba, D. J. Alexander, M. L. Grossbeck and S. Jitsukawa, *J. Nuc. Mat*., **258-263** (1998) 1275.
28. P. Spatig, R. Schaublin, S. Gyger and M. Victoria, *J. Nuc. Mat*., **258-263** (1998) 1345.
29. R. Schaublin, P. Spatig and M. Victoria, *J. Nuc. Mat*., **258-263** (1998) 1350.
30. D. S. Gelles, P. M. Rice, S. J. Zinkle and H. M. Chung, *J. Nuc. Mat*., **258-263** (1998) 1380.
31. P. M. Rice and S. J. Zinkle, *J. Nuc. Mat*., **258-263** (1998) 1414.
32. J. Gazda, M. Meshii and H. M. Chung, *J. Nuc. Mat*., **258-263** (1998) 1437.
33. E. V. van Osch and M. I. De Vries, *J. Nuc. Mat*., **271 & 272** (1999) 162.
34. Y. Candra, K. Fukumoto, A. Kimura and H. Matsui, *J. Nuc. Mat*., **271 & 272** (1999) 301.
35. D.H. Xu, B.D. Wirth, M.M. Li, and M.A. Kirk, *Acta Mater.* **60** (2012) 4286–4302

36. C.J. Ortiz and M.J. Caturla, *Phys. Rev. B* **75 (2007)**184101
37. C.J. Ortiz, P. Pichler, T. Fuhner, F. Cristiano, B. Colombeau, N.E.B. Cowern, and A. Claverie, *J. Appl. Phys.* **96** (2004) 4866–4877.
38. D. Xu and B.D. Wirth, *Fusion Sci. Technol.* **56** (2009) 1064–1068
39. D. Xu and B.D. Wirth, *J. Nucl. Mater.* **403** (2010) 184–190
40. D. Xu, X. Hu and B.D. Wirth, *Appl. Phys. Lett.* **102** (2013) 011904
41. X. Hu, D. Xu, T.S. Byun, and B.D. Wirth, *Modeling and Simulation in Materials Science & Engineering* **22** (2014) 0655002.
42. M.V. Smoluchowski, *Z. Physik Chem* **92** (1917) 192.
43. T.R. Waite, *Phys. Rev. B* **107** (1957) 463-470.
44. H.L. Heinisch, B.N. Singh and S.I. Golubov, *J. Nucl. Mater.* **283** (2000) 737.
45. H.L. Heinisch, H. Trinkaus and B.N. Singh, *J. Nucl. Mater.* **367** (2007) 332.
46. P. Erhart and J. Marian, *J. Nucl. Mater.* **414** (2011) 426.
47. R. E. Stoller, S. I. Golubov, C. Domain, and C. S. Becquart, *J. Nucl. Mater.* **382** (2008) 77.
48. D. Xu, B.D. Wirth, M. Li, and M. A. Kirk, *Applied Physics Letters* **101** (2012) 101905.
49. J.F. Ziegler, J.P. Biersack and U. Littmark, *The Stopping and Range of Ions in Matter* (Pergamon, New York, 1984).
50. P.M. Derlet, D. Nguyen-Manh and S.L. Dudarev, *Phys. Rev. B* **76** (2007) 054107.
51. B. Bortz, M.H. Kalos and J.L. Lebowitz, *J. Comp. Phys.* **17** (1975) 10.
52. D. Xu, B.D. Wirth, M. Li, and M.A. Kirk, *Current Opinion in Solid State Materials Science* **16** (2012) 109-114.
53. M. Li, M.A. Kirk, P.M. Baldo, D. Xu, and B.D. Wirth, *Phil Mag* **92(no. 16)** (2012) 2048-2078.
54. C.H. Woo and B.N. Singh, *Phil. Mag. A* **65** (1992) 889.
55. K. Arakawa, K. Ono, M. Isshiki, K. Mimura, M. Uchikoshi, and H. Mori, *Science* **318** (2007) 956.
56. A.H. Cottrell, *Proceedings of the Physical Society* **62** (1949) 49-62
57. M. Eldrup, B.N. Singh, S.J. Zinkle, T.S. Byun, and K. Farrell, *J. Nucl. Mater.* **307-311** (2002) 912–917.
58. S.J. Zinkle and B.N. Singh, *J. Nucl. Mater.* **351** (2006) 269–284.
59. M. Hernandez-Mayoral, Z. Yao, M. L. Jenkins, and M. A. Kirk, *Philos. Mag*. **88** (2008) 2881.
60. Z. Yao, M. Hernandez-Mayoral, M. Jenkins, and M. Kirk, *Philos. Mag.* **88** (2008) 2851 (2008).
61. Z. Yao, M. Jenkins, M. Hernandez-Mayoral, and M. Kirk, *Philos. Mag.* **90** (2010) 4623.
62. C. Topbasi, A. T. Motta, and M. A. Kirk, *J. Nucl. Mater.* **425** (2012) 48.
63. D. Kaoumi, J. Adamson, and M. Kirk, *J. Nucl. Mater.* **445** (2014) 12.
64. M. A. Kirk, P. M. Baldo, A. C. Liu, E. A. Ryan, R. C. Birtcher, Z. Yao, S. Xu, M. L. Jenkins, M. Hernandez-Mayoral, D. Kaoumi, and A. T. Motta, *Microscopy Research and Technique* **72** (2009) 82.
65. M. Jenkins, Z. Yao, M. Hernndez-Mayoral, and M. Kirk, *J. Nucl. Mater.* **389** (2009) 197.
66. M. L. Jenkins, C. A. English, and B. L. Eyre, *Philos. Mag. A* **38** (1978) 97.
67. C. Topbasi, "Microstructural Evolution Of Ferritic-martensitic Steels Under Heavy Ion Irradiation", *Ph.D. thesis*, Pennsylvania State University (2014).
68. Y. Satoh and H. Matsui, *Philos. Mag.* **89** (2009) 1489.
69. T. Hamaoka, Y. Satoh, and H. Matsui, *J. Nucl. Mater.* **433** (2013) 180.

70. K. Arakawa, H. Mori, and K. Ono, *J. Nucl. Mater.* **307-311** (2012) 272.
71. A.A. Kohnert and B.D. Wirth, manuscript submitted to *Phys. Rev. B* (2014).
72. A.A. Kohnert, "The kinetics of dislocation loop formation in ferritic alloys through the aggregation of irradiation induced defects", *PhD Thesis*, University of California, Berkeley (2014).
73. C. C. Fu, J. D. Torre, F. Willaime, J. L. Bocquet, and A. Barbu, *Nature Mat.* **4** (2005) 68.
74. C. C. Fu, F. Willaime, and P. Ordejon, *Phys. Rev. Lett.* **92** (2004) 175503.
75. A.V. Barashev, S.I. Golubov, Y.N. Osetsky, and R.E. Stoller, *Phil. Mag.* **90** (2010) 897-906.

Table 1. Optimized mobility set for interstitial clusters/loops and single vacancy in Molybdenum.

	$I_{n>20}$	$I_{11\sim20}$	$I_{1\sim10}$	V
D_0 (nm^2/sec)	$2\times10^{11}n^{-0.7}$	2×10^{11}/n		2×10^{11}
E_m (eV)	1.1	Linear-space (0.1 to 0.8)	0.1	0.9

Table 2. Mobility set for interstitial clusters/loops (*b*=1/2<111>) and single vacancy for the modeling of neutron irradiated (nominally) pure iron.

Cluster	V	$I - I_7$	I_8	I_9	I_{10}	I_{11}	I_{12}	I_{13}	I_{14}	I_{15}	$I_{n>15}$
E_m (eV)	0.75	0.34	0.45	0.50	0.55	0.65	0.75	0.80	0.9	0.95	1.1
D_0(nm^2/s)	1.37×10^{11}					1.37×10^{11}/n					$1.37\times10^{11}n^{-0.7}$

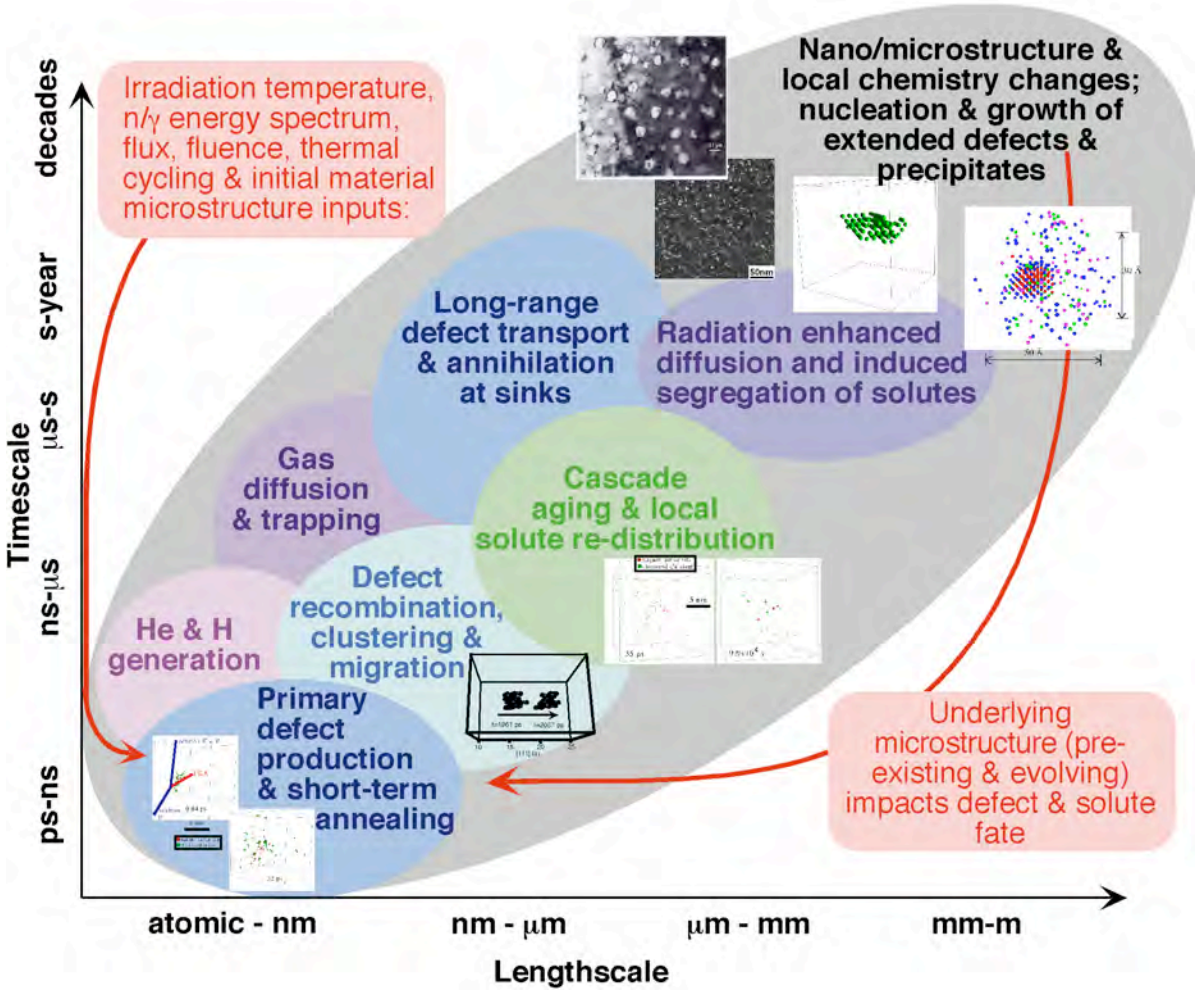

Figure 1 – Illustration of the length and time scales (and feedback) involved in the multiscale processes responsible for microstructural changes in irradiated materials.

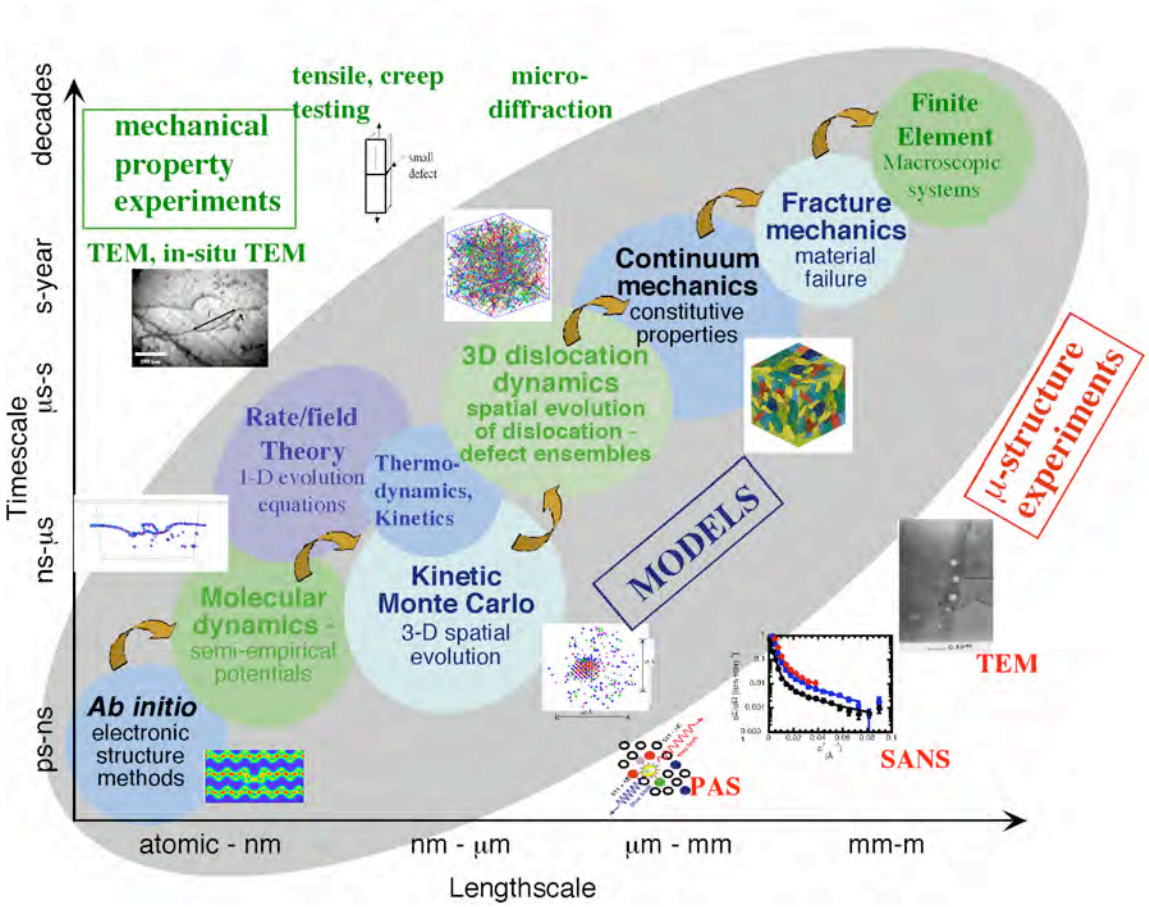

Figure 2 – Illustration of an integrated experimental and computational science-based approach to the multiscale investigation of materials degradation due to high-energy particle irradiation.

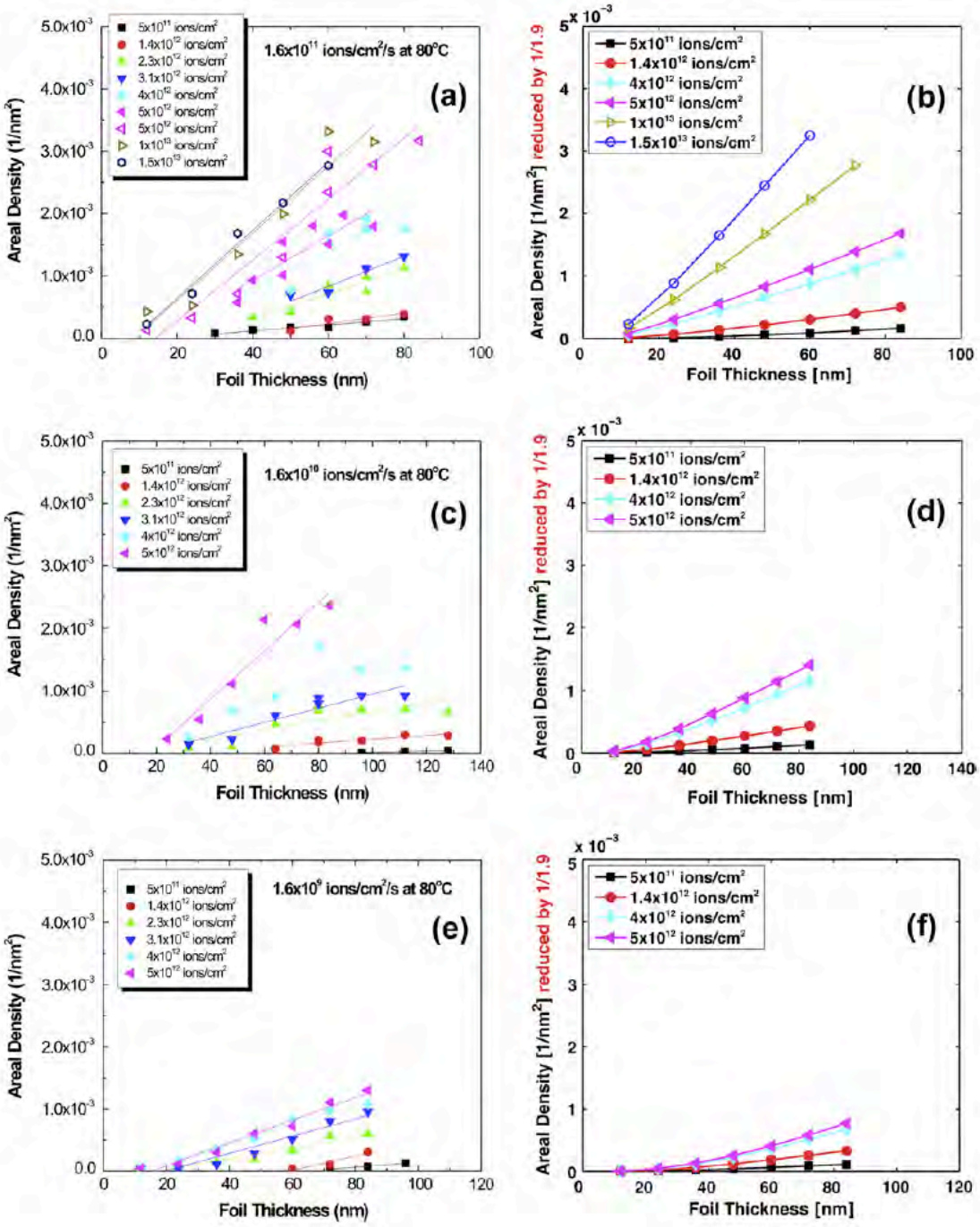

Figure 3. Experimental (a, c and e) and model-predicted (b, d and f) areal density of observed loops (size greater than 1.3 nm) in Molybdenum foils of varying thickness which were irradiated with 1 MeV Kr ions to a specified flux and fluence at temperature of approximately 80°C.

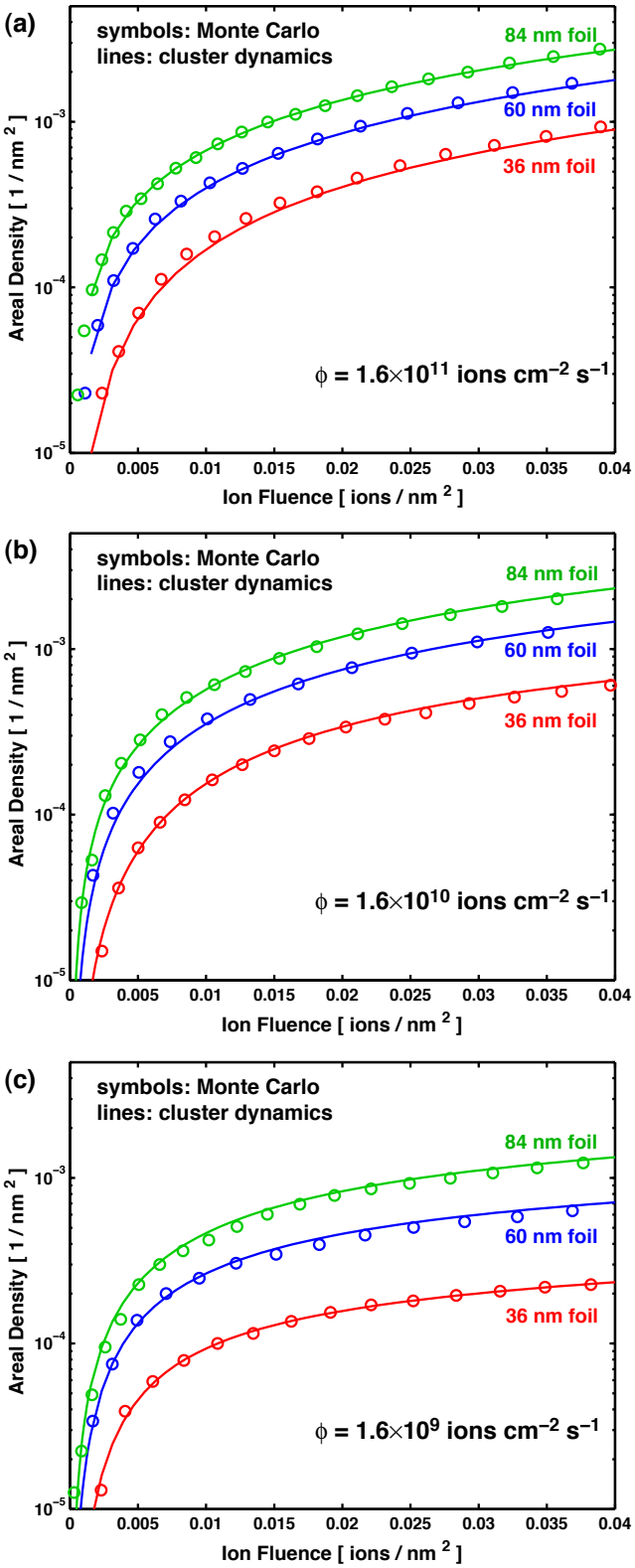

Figure 4. Comparison of areal density of visible defects from OKMC (open symbols) versus the CD model (solid lines) for three different foil thickness at three ion flux levels, (a) $1.6x10^{11}$, (b) $1.6x10^{10}$ and (c) $1.6x10^{9}$ ions/cm^2/sec.

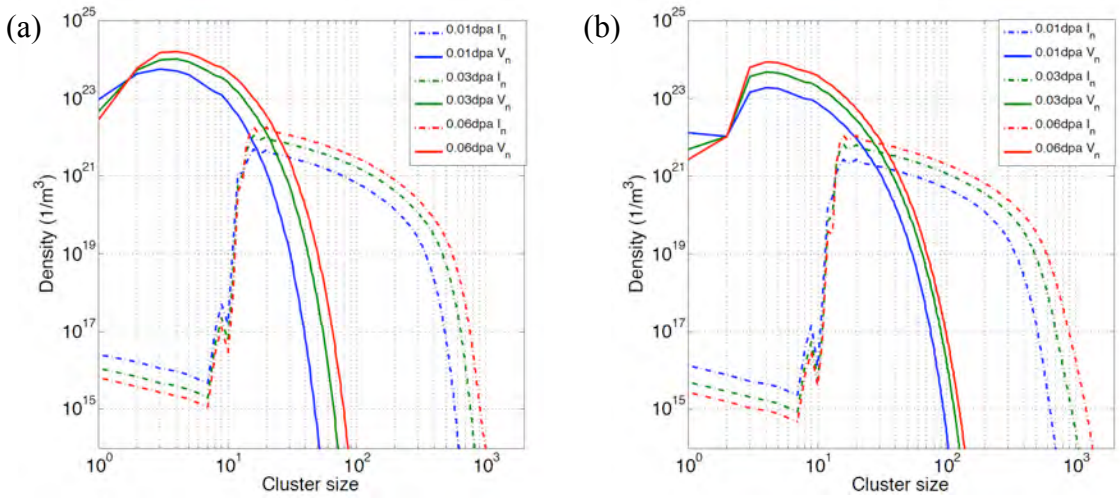

Figure 5. Volumetric density of interstitial (solid) and vacancy (dashed) clusters predicted by CD model as a function of cluster size (n, # of point defects contained in the cluster) at (a) 60°C and (b) 100°C, as a function of neutron dose (0.01, 0.03 and 0.06 dpa as blue, green and red, respectively).

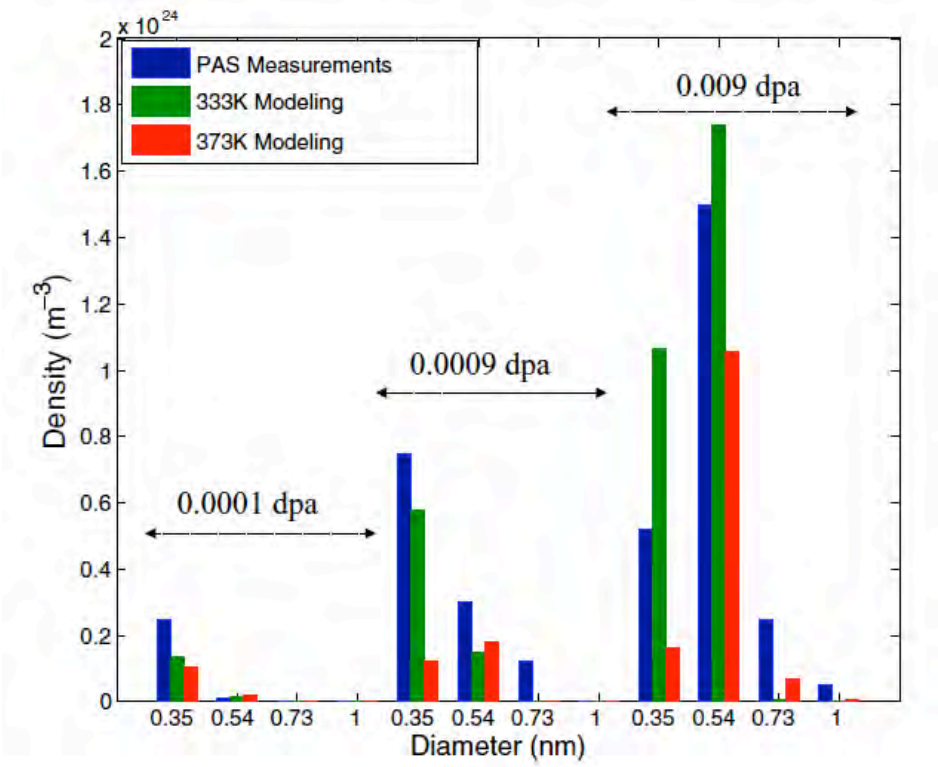

Figure 6. Comparison of modeling predictions (at 60 and 100°C in green and red, respectively) versus experimental positron measurements of the vacancy cluster size distribution in neutron irradiated iron, as a function of dose in dpa.

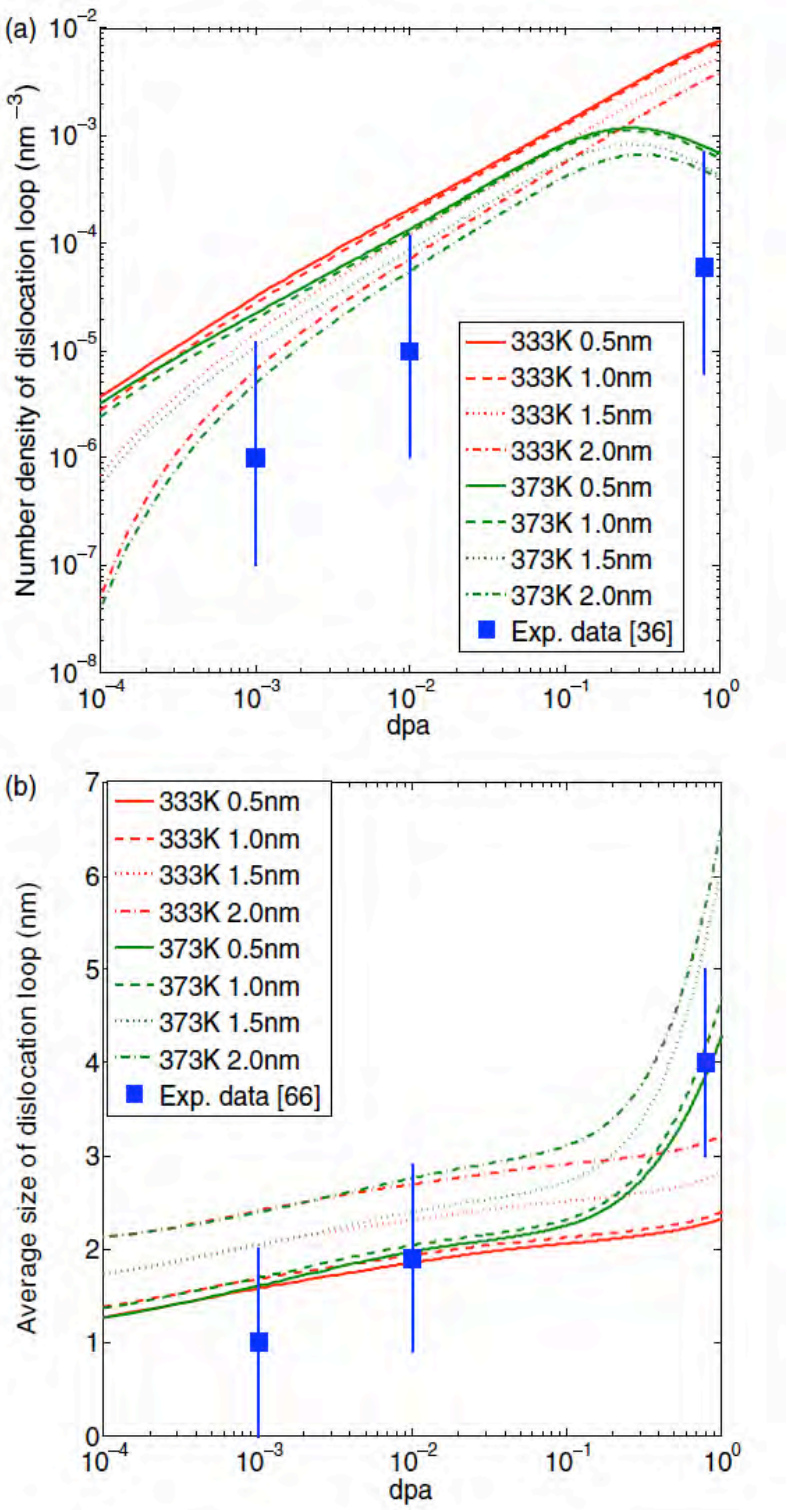

Figure 7. Comparison of Cluster dynamics modeling predictions of (a) interstitial-type dislocation loop density and (b) average size of the visible dislocation loop for 4 different TEM resolution limits (0.5 nm, 1.0 nm, 1.5 nm, and 2.0 nm) at two different neutron irradiation temperatures for the Fe-a samples, as compared to the TEM observations of Ref. [36, 68].

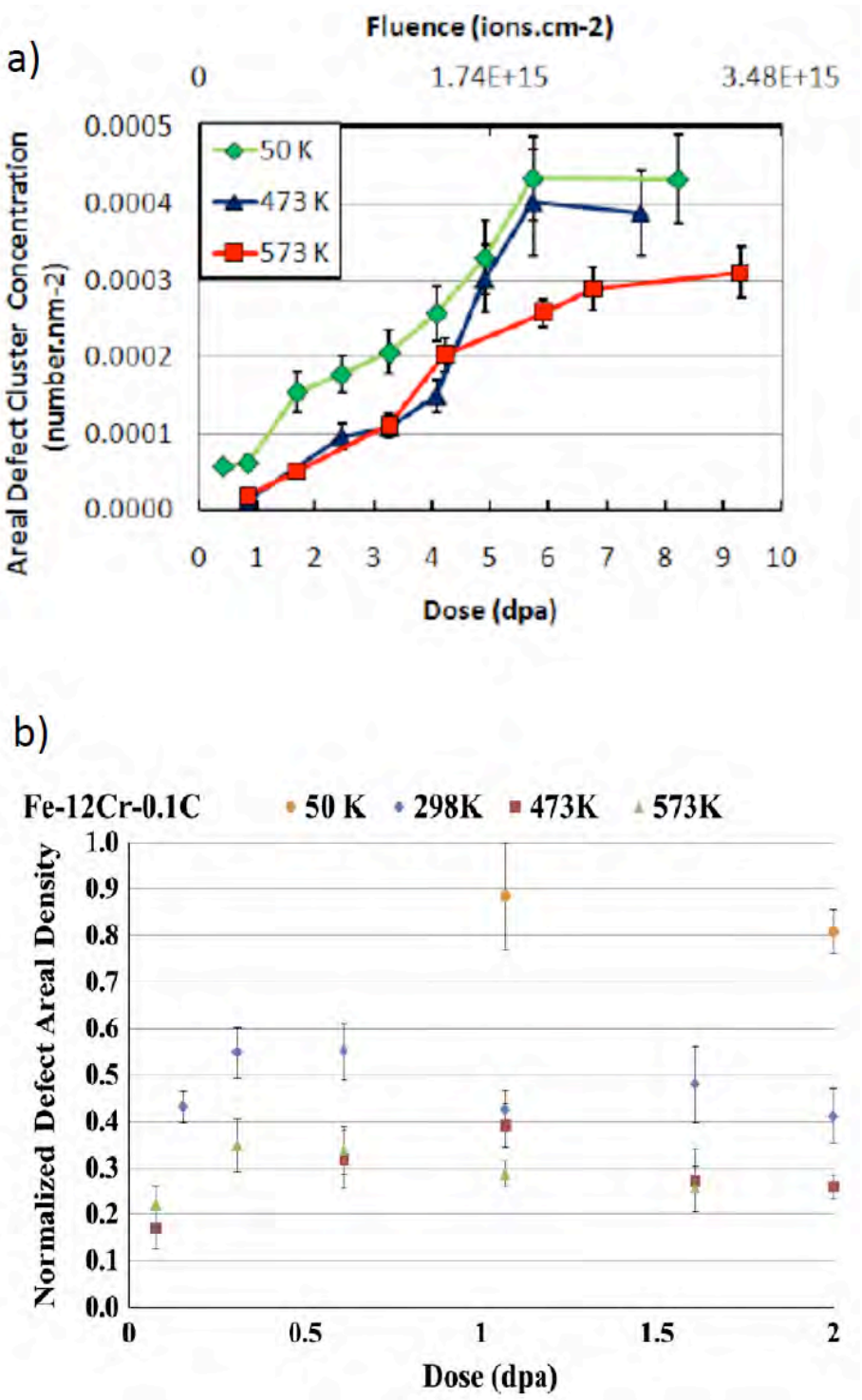

Figure 8. Temperature dependence of the areal defect density as a function of radiation dose for 1 MeV Kr ion irradiation of (a) commercial alloy NF616 [62,67] and (b) a model ferritic-martensitic steel with nominal composition of Fe-12Cr-0.1C [63].

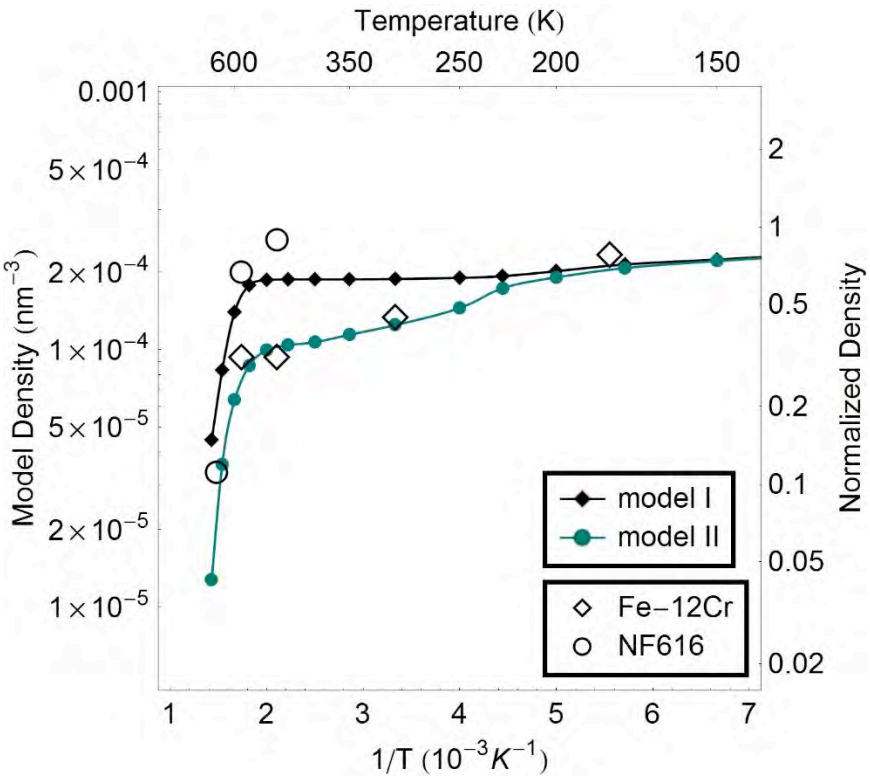

Figure 9. Predicted saturation density of visible defect clusters for 1 MeV Kr ion irradiation of ferritic-martensitic alloys from the CD model with beam activated diffusion implemented in the form of Eq. (11). The experimental data from Fig. 8 [62, 63, 67] are shown for comparison, as normalized to the defect density at 50K.

U.S. DEPARTMENT OF ENERGY

Nuclear Energy

Microstructural evolution in advanced structural materials under long-term and elevated temperature irradiation: a combined materials modeling and experimental investigation

OVERVIEW

Purpose: Further develop and evaluate mesoscale modeling techniques, including kinetic Monte Carlo and spatially dependent cluster dynamics for multiscale modeling. Report on most promising coarse-graining, or up-scaling, techniques

Objectives: Develop Multiscale Modeling Methodology and Validation Problems

Predicting materials performance in extreme irradiation environments with limited available nuclear reactor testing infrastructure necessitates development of scientific-based modeling approaches

Logical Path:

Research task	Year 1 Q1 Q2 Q3 Q4	Year 2 Q1 Q2 Q3 Q4	Year 3 Q1 Q2 Q3 Q4	Year 4 Q1 Q2 Q3 Q4
Task 1. Develop & document well characterized microstructural evolution test problems & experimental validation data across a range of temperature, dose and dose rate regimes and different geometries (e.g., thin film in situ and bulk neutron, electron or ion irradiation studies)				
Task 2. Develop (as necessary) and perform simulations of microstructural evolution to benchmark against the test problems:				
Task 2a. Kinetic Monte Carlo				
Task 2b. Spatially-dependent cluster dynamics				
Task 2c. Phase field				
Task 3. Cross comparison of modeling results and experimental data, including refinement of models & data of defect production and interaction kinetics				
Task 4. Definition of optimized modeling approaches for coarse-graining micro- and mesoscale modeling to integrated materials performance codes of microstructural evolution				

Outcomes: Develop well-posed, experimental validation test problems & enable efficient, multiscale materials modeling of materials performance in nuclear environments

DETAILS

Principal Investigator: Brian Wirth

Institution: University of Tennessee

Collaborators:N/A

Duration: 4 years **Total Funding Level:** $750K

TPOC: Xin Sun

Federal Manager: Rob Versluis

Workscope: ARC-3

PICSNE Workpackage #:
CFP-11-2979

RESULTS

Figure shows a comparison of cluster dynamics model predictions of thin film irradiation experiments in two Fe-Cr based ferritic martensitic alloys, as a function of temperature, with different sets of kinetic properties

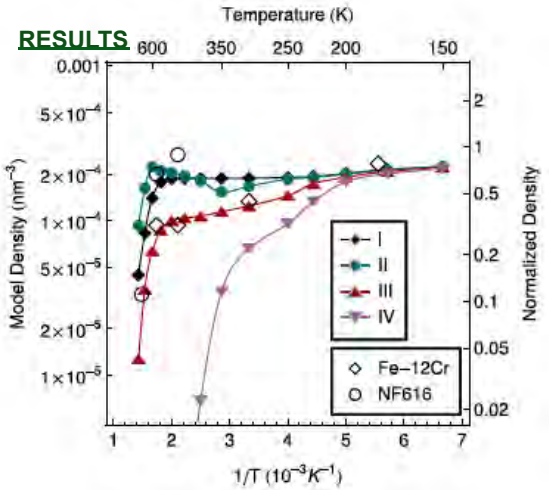

Accomplishments:

BD Wirth, X. Hu, A. Kohnert, and D. Xu, "Modeling Defect Cluster Evolution in Irradiated Structural Materials: Focus on comparing to high-resolution experimental characterization studies", *Journal of Materials Research* **30** (2015) 1440-1455.